Boundary layer effects in droplet splashing

Guillaume Riboux and José Manuel Gordillo
Área de Mecánica de Fluidos, Departamento de Ingeniería Aeroespacial y Mecánica de Fluidos, Universidad de Sevilla, Avenida de los Descubrimientos s/n 41092, Sevilla, Spain.

A drop falling onto a solid substrate will disintegrate into smaller parts when its impact velocity, V, exceeds the so called critical velocity for splashing, i.e., when $V > V^*$. Under these circumstances, the very thin liquid sheet ejected tangentially to the solid after the drop touches the substrate, lifts off as a consequence of the aerodynamic forces exerted on it. Subsequently, the growth of capillary instabilities break the toroidal rim bordering the ejecta into smaller droplets, violently ejected radially outwards, provoking the splash [1]. In this contribution, the effect of the growth of the boundary layer is included into the splash model presented in [1], obtaining very good agreement between the measured and the predicted values of V^* for wide ranges of liquid and gas material properties, atmospheric pressures and substrate wettabilities. Our new description also modifies the way the instant of time at which the liquid sheet is first ejected, which can now be determined in a much more straightforward manner than that proposed in [1].

I. INTRODUCTION

Current technological applications such as coating, cleaning, cooling, combustion, microfabrication through droplet deposition or the generation of aerosols, require a precise knowledge of the conditions under which a drop hitting a solid substrate, either conserves its integrity after the impact, or disintegrates into smaller parts [2]. The relevance of droplet splashing in many natural and engineering processes, and even in forensic sciences [3], together with the advances produced in high speed imaging [2], have stimulated the appearance, during the past twenty years, of a vast number of experimental, numerical and theoretical studies on the subject [4–18]. It is our purpose here to improve the agreement between the critical velocities for splashing predicted by the model presented in [1] with the experimental data. It has been recently reported that the model in [1], R&G in what follows, is able to quantitatively predict V^*, namely, the critical velocity for splashing, in a wide variety of experimental conditions [19–21], being this the reason why we believe that the improvements to the R&G model described here could be useful for researchers working on the description of droplet splashing. Here, we will only refer to the problem of splashing caused by the impact of a drop onto a solid substrate, being the analogous physical situation of drop splashing by impact onto a liquid film, the subject of other recent contributions [22–27], to which the interest reader is directed.

The starting point of the model proposed by R&G is to determine the ejection time of the lamella T_e, as well as the initial values of the thickness and the velocity of the edge of liquid sheet, $H_t(T = T_e)$ and $V_t(T = T_e)$ (see Figure 1). Following R&G, R, V, R/V and ρV^2 are, respectively, the characteristic length, velocity, time and pressure used to define the different dimensionless variables, written in lowercase letters to differentiate them from their dimensional counterparts. Here, R indicates the droplet radius, V is the impact velocity and ρ is the liquid density. Some of the main findings in R&G can be summarized as follows:

1. The radius of the circular wetted area illustrated in Figure 1 evolves in time as $a = \sqrt{3t}$ (see R&G).

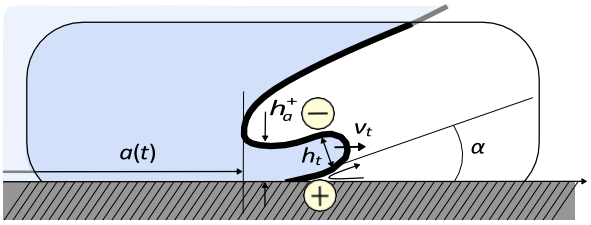

FIG. 1. (color online) Sketch of the lamella for $T > T_e$ for $V > V^*$ i.e., for impact velocities above which the lamella dewets the substrate. The regions in which the pressure is larger or smaller than the reference atmospheric pressure are indicated with either a plus or a minus sign. The lift force responsible of droplet splashing results from the integration of the pressure distribution along the edge of the lamella. This figure also illustrates the definitions of the different variables needed to describe the position of the rim.

2. The velocity at which the lamella is initially ejected is $v_t(t_e) = \dot{a}(t_e) = 1/2\sqrt{3/t_e}$, with dots denoting time derivatives.

3. The thickness of the edge of the lamella at the instant of ejection is $h_t \propto h_a = 2t^{3/2}/(\sqrt{3\pi})$ (see the supplementary material in R&G).

4. Since $\dot{a} = v_t$ at $t = t_e$ and the lamella can only be ejected if its tip advances faster than $\dot{a}$, t_e is calculated imposing that the deceleration of the edge of the lamella, $\dot{v}_t$, coincides with the deceleration of the wetted area, $\ddot{a}$.

In R&G, the ejection time, which is determined imposing the condition $\dot{v}_t = \ddot{a}$, yields the following equation for t_e:

$$c_1 \mathrm{Re}^{-1} t_e^{-1/2} + \mathrm{Re}^{-2}\mathrm{Oh}^{-2} = \ddot{a} h_t^2 = c^2 t_e^{3/2}, \qquad (1)$$

where $\mathrm{Re} = \rho V R/\mu$ and $\mathrm{Oh} = \mu/\sqrt{\rho R \sigma}$ denote, respectively, the impact Reynolds and Ohnesorge numbers, σ is the interfacial tension coefficient and $c_1 \times 3/2$ and $c = 1.1$ are constants adjusted experimentally; the Weber number is defined here as $\mathrm{We} = \rho V^2 R/\sigma = \mathrm{Re}^2\,\mathrm{Oh}^2$. Equation (1) expresses that, in the limit $\mathrm{Oh} \ll 1$, $t_e \propto \mathrm{We}^{-2/3}$, whereas,

	λ_0 ($\times 10^{-9}$ m)	μ_g ($\times 10^5$ Pa s)	ρ_{g0} (kg m^{-3})
Helium	180	1.98	0.16
Air	65	1.85	1.18
Krypton	55	2.51	3.42
SF_6	39	1.53	6.04

TABLE I. Physical properties of the gases used in the experiments of Figure 9(b) for $T_{g0} = 298.15$ K and $p_{g0} = 10^5$ Pa. Therefore, for arbitrary values of the gas temperature T_g and pressure p_g, $\lambda = \lambda_0\ (T_g/T_{g0})\ (p_{g0}/p_g)$ and $\rho_g = \rho_{g0}\ (T_{g0}/T_g)\ (p_g/p_{g0})$.

in the moderate to high values of the Ohnesorge number, $t_e \propto \mathrm{Re}^{-1/2}$. We also demonstrate in the supplementary material of R&G that, under the potential flow assumption and, for impact velocities such that $V > V^*$, the thickness of the lamella and the liquid velocity at $r = 3t$ i.e., at the radial position where the drop intersects the substrate, are respectively given by

$$h_a = 2\,t^{3/2}/(\sqrt{3}\pi) \quad \text{and} \quad v_a = \sqrt{3/t}. \tag{2}$$

Equations (2) were also deduced in [28] in a rather different way to that followed in R&G for the analogous case of the entry of a solid object into a liquid [29–33].

In R&G it is also shown that, once the sheet is ejected, its edge experiences a *vertical* lift force per unit length

$$F_L = K_l \mu_g\, V_t + K_u\, \rho_g\, V_t^2\, H_t, \tag{3}$$

which results from the addition of the lubrication force exerted by the gas in the wedge region located between the advancing lamella and the substrate -see Figure 1-, $K_l \mu_g V_t$, and the suction force exerted by the gas at the top part of it, $K_u\, \rho_g\, V_t^2\, H_t$ [1]. Here, the subscript g represents gas quantities, $K_u \times 0.3$ is a constant determined numerically and K_l is deduced using lubrication theory once it is assumed that the front part of the advancing liquid sheet can be approximated to a wedge of constant angle $\alpha \times 60^\circ$ while it is in contact with the substrate. The origin of the constant wedge angle α, relies on the fact that the no slip condition provokes the edge of the liquid sheet to be convected further downstream than the region in contact with the solid, being this argument in agreement with the experimental observations in [20], where it is also reported that the substrate wettability does not appreciably affect the splash threshold velocity through α.

The coefficient K_l in (3) is deduced using lubrication theory in the supplementary material of R&G, yielding

$$K_l = -(6/\tan^2\alpha)\ C_2\, a \ln(1+a) - a \ln a + C_3\, b \ln(1+b) - b \ln b \quad , \tag{4}$$

with

$$a = 2\ \bar{l}_g + \bar{l}_\mu\ + 2\sqrt{\bar{l}_g - \bar{l}_\mu\ ^2 + \bar{l}_g \bar{l}_\mu}$$
$$b = 2\ \bar{l}_g + \bar{l}_\mu\ - 2\sqrt{\bar{l}_g - \bar{l}_\mu\ ^2 + \bar{l}_g \bar{l}_\mu}\ . \tag{5}$$

The different coefficients in (4) and the dimensionless variables in (5) are defined as

$$C_1 = \frac{2\,\bar{l}_\mu}{a\,b}, \quad C_2 = \frac{1 - C_1\, b}{b - a}, \quad C_3 = -(C_1 + C_2), \tag{6}$$
$$\bar{l}_\mu = l_\mu/H_0 \quad \text{and} \quad \bar{l}_g = l_g/H_0\ .$$

Here, $H_0 = H_t/4$, $l_g \times 1.2\lambda$ is the slip length of the gas [34], $\lambda = k_B\, T_g/(\sqrt{2}\pi d^2 p_g)$ is the mean free path between gas molecules, k_B is Boltzmann constant, T_g and p_g are the gas temperature and pressure respectively, and d indicates the effective diameter of gas molecules -values of λ, μ_g and ρ_g for different gases are provided in Table I- Differently to R&G, where $\bar{l}_\mu$ in equation (5) was set to zero, yielding

$$K_l = -(6/\tan^2(\alpha))\ (\ln[8 l_g/H_t] - \ln[1 + 8 l_g/H_t])\ , \tag{7}$$

here, we will retain the complete expression of K_l given by (4), with $l_\mu = H_t\, \mu_g/\mu$ (see the supplementary material in [1] for details).

The vertical velocity at which the lamella is *initially* expelled, $V_v(T_e)$, can be deduced from the force balance projected in the vertical direction, $\rho_t H^2 \dot{V} \propto F_L = K_u\, \rho_g\, V_t^2 + K_l\, \mu_g\, V_t$, from which it can be deduced that

$$V_v(T_e) \propto \sqrt{F_L/(\rho\, H_t)}\ . \tag{8}$$

The splash criterion in [1], results from imposing that the vertical velocity (8) is such that $\beta = V_v/V_{TC}$ with $V_{TC} = \sqrt{2\sigma/\rho\, H_t}$ the capillary retraction velocity [35, 36] and $\beta \times 0.14$.

Equation (4) reveals that the lift force exerted by the lubrication layer located beneath the advancing front, depends logarithmically on the ratio λ/H_t, with λ mean free path of the gas. It will be shown below that the ratio λ/H_t could be of order unity or even larger, being this the reason why the splash threshold velocity is sensitive to small changes of H_t. Motivated by this fact and, in order to account for the effect of the boundary layer developing upstream the ejected liquid sheet, the equations for the ejection time (1) and for the thickness of the lamella, H_t, will be slightly changed with respect to the corresponding expressions derived in R&G.

II. INFLUENCE OF THE BOUNDARY LAYER ON THE EJECTION TIME

The large values of the Reynolds number characterizing the splashing of a droplet impacting against a wall suggests to describe the tangential deceleration of the fluid at the solid substrate by means of boundary layer theory. As a first step, the results of the type of simulations describing the impact of a drop against a shear free wall described in [37] and illustrated in Figures 2(a)–(b), provide the velocity field at the solid substrate for different instants of time: the radial velocity field computed using potential flow theory corresponds to the far field boundary condition for the velocity component tangent

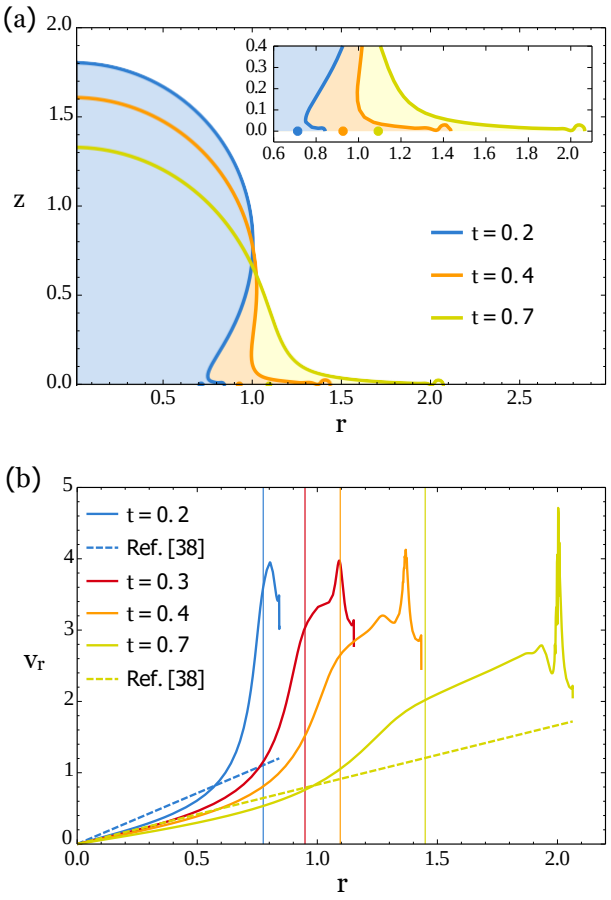

FIG. 2. (color online) (*a*) Computed shapes of a drop using the potential flow numerical code described in [37] for a value of the Weber number We = 100. The inset indicates the position of the stagnation point existing in the flow in a relative frame of reference translating with a velocity $a^{\cdot}$ for different instants of time. (*b*) Comparison between the computed values of the radial velocity $v_r(r, z = 0)$ corresponding to the different drop shapes depicted in figure (*a*) (continuous lines) and the radial velocity field assumed ad hoc in [38] (dashed lines). The origin $r = 0$ corresponds to the impact point. The vertical lines indicate the radial position of the root of the lamella, $r = a = \sqrt{3t}$.

to the solid, v_r, in the boundary layer equations. Interestingly, Figure 2(*b*) reveals that the stagnation-point type of flows used in previous studies [38–40], are in clear disagreement with the real ones. More precisely, Figure 2(*b*) reveals that, in the neighborhood of the spatial region from which the lamella is ejected, $r = a(t) = \sqrt{3t}$, the computed radial velocity at $z = 0$ is much larger than the corresponding velocity corresponding to a stagnation-point type of flow, $v_r \approx r/t$. This analytical form of the radial velocity, $v_r \approx r/t$, is used, for instance, in references [38–40]; it will also be shown below that the relevant outer velocity field for the development of the boundary layer flow entering the ejected thin liquid sheet is not the one considered in [17, 41] either.

Indeed, Figure 3(*a*) represents the radial velocity field computed using potential flow simulations [37] in a frame of reference moving at $\dot{a}$, namely, the speed at which the root of the lamella, located at $r = a$, propagates radially. Interestingly enough, Figure 3(*a*) shows that, in agreement with potential flow theory [28, 30–32] and by virtue of the Euler-Bernoulli equation applied in the moving frame of reference [1], the velocity entering into the lamella in the moving frame of reference is $a^{\cdot}$ *once the lamella is ejected* i.e., the velocity of fluid particles entering into the lamella is $2a^{\cdot}$ in the fixed frame of reference. Figure 3(*a*) also indicates that fluid particles entering into the lamella come from a very narrow region, located between $r = r_s$, which is the radial position of the stagnation point of the flow in the moving frame of reference, and the root of the lamella. Therefore, the relevant spatial region to describe the boundary layer flow of interest here, is the one located between $r_s < r < \sqrt{3t}$, where radial velocity field computed using potential flow theory [37], notably differs from that assumed in previous studies [17, 38–41], as it will be shown below.

First, Figure 3(*b*) shows that $\sqrt{3t} - r_s(t) = c_n\, h_a(t) \propto t^{3/2}$, with $c_n = 1.5$, a result which is consistent with equation (6) for the velocity in the relative frame of reference provided in the supplementary material of [1]

$$\boldsymbol{v}_r - a^{\cdot}\,\boldsymbol{e}_x = -\frac{\sqrt{2a}}{\pi\sqrt{a-r}}\,\sin(\vartheta/2)\,\mathbf{e}_r + \cos(\vartheta/2)\,\mathbf{e}_\vartheta - a^{\cdot}\,\mathbf{e}_x, \tag{9}$$

from which it can be deduced that

$$(a - r_s)^{-1/2}\,\frac{\sqrt{2a}}{\pi} = a^{\cdot} \Longrightarrow (a - r_s) = \frac{4}{\pi^2} h_a^2, \tag{10}$$

Figure 4 shows that, in agreement with equation (9), the radial velocity in the fixed frame of reference varies with the distance to the root of the lamella as $(a - r)^{-1/2}$ for $r \times r_s$ and, even more interestingly, Figure 4 shows that the radial velocity field for $r_s(t) < r < a(t)$ can be well approximated by

$$v_{ext} \times a^{\cdot}\left(1 + \frac{r - r_s}{c_n\, h_a}\right), \tag{11}$$

with $c_n = 1.5 \approx 4/\pi$, see Figure 3(*b*) and equation (10). Due to the fact that in the spatial region $r_s < r < a$, $v_r/r \sim v_r/a$ and $\partial v_r/\partial r \sim v_r/h_a$, it can be deduced that, for $t \gg 1$, $v_r/r \ll \partial v_r/\partial r$ because $a(t) \gg h_a(t)$ ($a \propto t^{1/2}$ and $h_a \propto t^{3/2}$). Therefore, the continuity and momentum equations describing the radial and normal components of the velocity field within boundary layer developing in the spatial region $r_s < r < a$ can be simplified to

$$\begin{aligned} &\frac{\partial V_r}{\partial X} + \frac{\partial V_z}{\partial Z} = 0, \\ &V_r\frac{\partial V_r}{\partial X} + V_z\frac{\partial V_r}{\partial Z} = V_{ext}\frac{\mathrm{d}V_{ext}}{\mathrm{d}X} + \nu\frac{\partial^2 V_r}{\partial Z^2}. \end{aligned} \tag{12}$$

In equation (12), the variable $X = R(r - r_s)$ has been defined to describe the boundary layer flow between $r_s = a - c_n\, h_a$ and $r = a = \sqrt{3t}$, $V_{ext} = V\dot{a}(1 + (r - r_s)/(c_n\, h_a))$ is

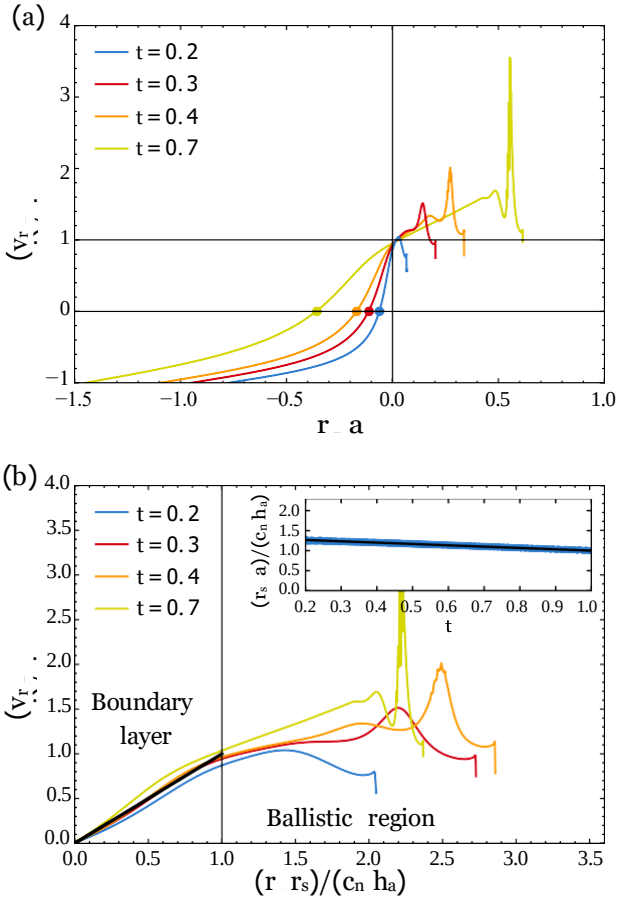

FIG. 3. (color online) (a) Time evolution of the values of the radial velocity profiles depicted in Figure 2(b) represented in a frame of reference translating at a velocity $a^{\cdot} = 1/2\ \ 3/t$. The values of the radial velocity are normalized by $a^{\cdot}$ and are represented as function of the distance to the root of the lamella, $r - a$. Notice that the relative radial velocity is $a^{\cdot}$ at $r = a$ and is zero at $r = r_s$, with r_s indicating the radial position of the stagnation point in the relative frame of reference, marked using a colored dot. (b) The radial velocity v_r varies linearly between $r = r_s$ and $r = a$, namely, the spatial region located between the stagnation point of the flow in the relative frame of reference and the root of the lamella. Indeed, notice that distances are normalized here by $r_s - a = c_n h_a(t)$, with $c_n = 1.5$ a constant (see the inset). The relevant region for the development of the boundary layer flow entering into the lamella is $0 < (r - r_s)/(c_n h_a) < 1$, whereas the region $(r - r_s)/(c_n h_a) > 1$ corresponds to that of the ejected liquid sheet, which can be described using a ballistic approximation [37, 42]

defined in equation (11) and the quasi steady Euler-Bernoulli equation has been used to compute the pressure gradient in the boundary layer region. Indeed, the local acceleration term has been neglected in the system (12) due to the fact that the residence time T_r of fluid particles in the spatial region $r_s < r < a$ is $T_r \sim Rh_a/(V\dot{a}) \sim (R/V)\,t^2$, whereas the characteristic time of variation of the flow field in this region is $T_0 \sim (R/V)\,t$. Consequently, since the process of droplet splashing described here takes place for $t \quad 1$, and $O(\partial V_r/\partial T) \sim (V\dot{a})/T_0$ and $O(V_r \partial V_r/\partial X) \sim$

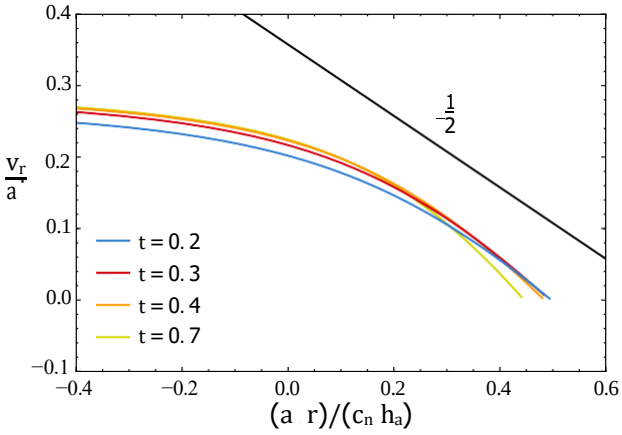

FIG. 4. (color online) Log-log plot of the radial velocity as a function of the distance to the root of the lamella. In agreement with equation (9), the radial velocity decays as $(a - r)^{-1/2}$ for r & r_s.

$V^2\dot{a}^2/(Rh_a)$, the order of magnitude of the ratio of the local and the convective acceleration terms in the momentum equation is $\sim T_r/T_0 \quad t \sim 1$ and, thus, the flow in the boundary layer region $r_s < r < a$ can be considered quasi-steady.

In terms of the new dimensionless variables

$$\bar{x} = \frac{X}{R\,c_n\,h_a},\ \bar{z} = \frac{Z}{R\,c_n\,h_a}\,(\mathrm{Re}\,c_n)^{1/2}\,(a^{\cdot}\,h_a)^{1/2},$$
$$\bar{v}_r = \frac{V_r}{V\dot{a}},\ \bar{v}_z = \frac{z}{V\dot{a}}\,(\mathrm{Re}\,c_n)^{1/2}\,(a^{\cdot}\,h_a)^{1/2}, \tag{13}$$

the system (12) reads

$$\frac{\partial \bar{v}_r}{\partial \bar{x}} + \frac{\partial \bar{v}_z}{\partial \bar{z}} = 0$$
$$\bar{v}_r \frac{\partial \bar{v}_r}{\partial \bar{x}} + \bar{v}_z \frac{\partial \bar{v}_r}{\partial \bar{z}} = 1 + \bar{x} + \frac{\partial^2 \bar{v}_r}{\partial \bar{z}^2}. \tag{14}$$

The system (14) describes the growth of a boundary layer within an outer potential flow which imposes a favorable pressure gradient: indeed, the pressure reaches a maximum at the stagnation point existing in the flow in the relative frame of reference, located at $r = r_s$, where $p = p_a + 1/2\rho V^2\dot{a}^2$ and pressure decreases downstream to match the atmospheric pressure, $p = p_a$ at the radial position from which the thin liquid sheet is ejected, $r \quad a$, see Figure 5.

The parabolic system of equations (12), which needs to be solved subjected to the following boundary conditions

$$\bar{x} = 0,\ \bar{v}_r = \bar{v}_{r0}(\bar{z})$$
$$\bar{z} = 0,\ \bar{v}_r = 0 \tag{15}$$
$$\bar{z} \to \infty,\ \bar{v}_r \to 1 + \bar{x}$$

admits a solution of the type

$$\bar{v}_r = (1 + \bar{x})\,\frac{df}{d\bar{z}}(\bar{z}),\ \bar{v}_z = -f(\bar{z}), \tag{16}$$

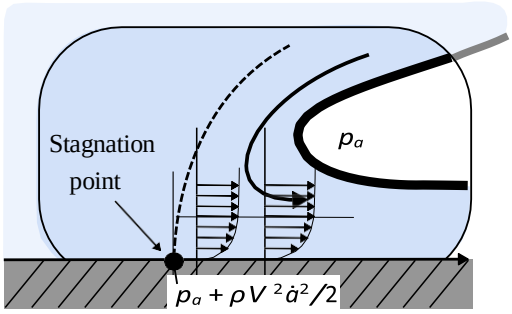

FIG. 5. (color online) Sketch of the flow developing between the stagnation point in the relative frame of reference and the root of the lamella.

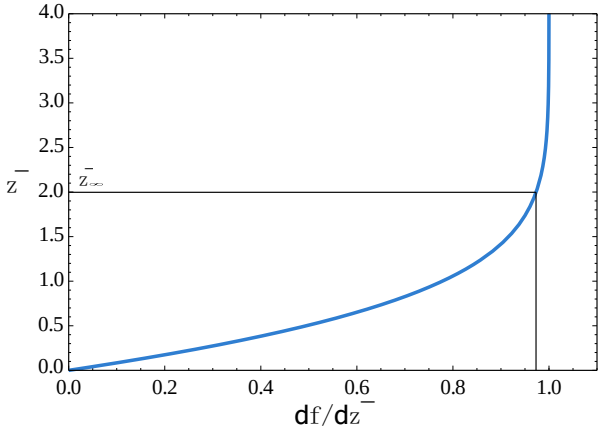

FIG. 6. (color online) Solution of equation (17) subjected to the boundary conditions given in equation (18).

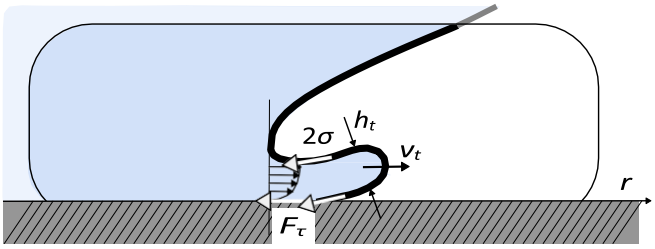

FIG. 7. (color online) Sketch of the forces decelerating the advancing front of the lamella.

with f given by the solution of the Falkner–Skan-type of equation [43]

$$\frac{d^3 f}{d\bar{z}^3} + 1 - \left(\frac{df}{d\bar{z}}\right)^2 + f\frac{d^2 f}{d\bar{z}^2} = 0, \tag{17}$$

satisfying the following boundary conditions

$$f(0) = \left.\frac{df}{d\bar{z}}\right|_0 = 0 \quad \text{and} \quad \bar{z} \to \infty, \quad \frac{df}{d\bar{z}} \to 1. \tag{18}$$

Since the system of equations is parabolic, the downstream evolution of the velocity profiles lose memory of the initial condition at $\bar{x} = 0$, a fact favoring the solution convergence to that provided by equation (17) [44]. The solution of equation (17) subjected to the boundary conditions (18), which is represented in Figure 6, reveals that the shear force per unit length F_τ exerted at the wall in the region $r_s < r < a$ and the thickness of the boundary layer δ, are respectively given by

$$\begin{aligned} F_\tau &= \mu \int_0^{R(a-r_s)} \left.\frac{\partial V_r}{\partial Z}\right|_{Z=0} dX \\ &= \frac{3}{2} c_n^{1/2} \left.\frac{d^2 f}{d\bar{z}^2}\right|_0 \mu V \,\mathrm{Re}^{1/2} \dot{a} (a \dot{h}_a)^{1/2} \\ &\quad \times 1.1 \mu V \,\mathrm{Re}^{1/2}, \end{aligned} \tag{19}$$

and

$$\begin{aligned} \frac{\delta}{R} &\times \bar{z}_\infty c_n^{1/2} \left(\frac{h_a}{\dot{a}}\right)^{1/2} \mathrm{Re}^{-1/2} \\ &\times 2.45 \left(\frac{h_a}{\dot{a}}\right)^{1/2} \mathrm{Re}^{-1/2}, \end{aligned}$$

where use of the values $\bar{z}_\infty \approx 2$ (see Figure 6), $c_n^{1/2} = \sqrt{3/2}$ and $d^2 f/d\bar{z}^2(0) = 1.23 \approx 3/2$ has been made.

Making use of the estimation of the boundary layer thickness in equation (19) and of equation (2), it can be concluded that, at the ejection time t_e,

$$\frac{\delta}{H_a} \times 4.34\,\mathrm{Re}^{-1/2} t_e^{-1/2}. \tag{20}$$

In the usual limit $\delta/H_a \ll 1$, the fluid within the ejected liquid sheet will be decelerated only by the action of interfacial tension forces. This assertion is true except in a very narrow region of thickness $\delta \ll H_a$ located nearby the wall, where viscous stresses also contribute to decelerate the liquid. Excluding the effect of this very thin region, the ejection condition $\dot{v}_t = \ddot{a}$ [1], with dv_t/dt the deceleration of the edge of the lamella sketched in Figure 7 reads,

$$\rho H_a^2 \dot{V}_T \sim -2\sigma \Longrightarrow \dot{v}_t \propto -\frac{\mathrm{We}^{-1}}{h_a^2}, \tag{21}$$

yielding the following expressions for both the ejection time and for the initial thickness of the lamella

$$\begin{aligned} &\dot{v}_t \propto -\mathrm{We}^{-1}/h_a^2 \propto \ddot{a} \\ &\Longrightarrow t_e \propto \mathrm{We}^{-2/3}, \quad h_a(t_e) \propto t_e^{3/2} \propto \mathrm{We}^{-1}. \end{aligned} \tag{22}$$

The scalings in (22), which have been verified numerically in [37], are valid only if

$$\begin{aligned} &\frac{\delta}{H_a} \times 4.34\,\mathrm{Re}^{-1/2} t_e^{-1/2} < 1 \\ &\Longrightarrow 4.34\,\mathrm{Re}^{-1/2}\,\mathrm{We}^{1/3} = 4.34\,\mathrm{Re}^{1/6}\,\mathrm{Oh}^{2/3} < 1 \\ &\Longrightarrow \mathrm{Re}^{1/6}\,\mathrm{Oh}^{2/3} \gtrsim 0.25, \end{aligned} \tag{23}$$

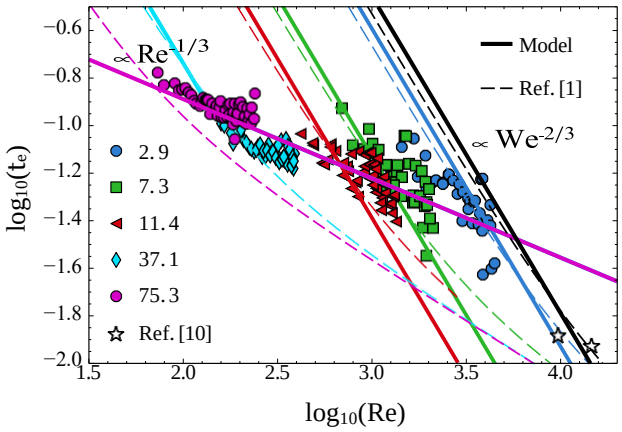

FIG. 8. (color online) Continuous lines represent the values of t_e calculated either as $t_e = 1.05\,\mathrm{We}^{-2/3}$ for $\mathrm{Re}^{1/6}\mathrm{Oh}^{2/3} < 0.25$ or as $t_e = 0.6\,\mathrm{Re}^{-1/3}$ for $\mathrm{Re}^{1/6}\,\mathrm{Oh}^{2/3} > 0.25$. Dashed lines represent the values of t_e obtained solving equation (1). The numerical values associated with each symbol represent 1000 Oh. The value of the Ohnesorge number is $\mathrm{Oh} = 2.3\times10^{-3}$ for the case of the experiments reported in [10].

where use of equations in (2), (20) and (22) has been made. In view of equation (22), the ejection time is given by $t_e \propto \mathrm{We}^{-2/3}$ if $\mathrm{Re}^{1/6}\mathrm{Oh}^{2/3} < 0.25$. However, when the thicknesses of the boundary layer is similar to that of the lamella, namely, $\mathrm{Re}^{1/6}\mathrm{Oh}^{2/3} \gtrsim 0.25$, fluid particles entering the ejected liquid sheet will also be decelerated by the action of the viscous shear force per unit length acting on a region of length $\sim H_a \sim F_\tau$ with F_τ calculated in equation (19) (see Figure 7). Consequently,

$$\begin{aligned} \rho H_t^2 \dot{V}_T &\propto -F_\tau - 2\sigma \\ &\propto -\mu V\,\mathrm{Re}^{1/2}\left(1+O\left(\mathrm{Re}^{-3/2}\,\mathrm{Oh}^{-2}\right)\right) \\ &\propto -\mu V\,\mathrm{Re}^{1/2} \\ \Rightarrow \dot{v}_t &\propto -\mathrm{Re}^{-1/2}/h_a^2. \end{aligned} \tag{24}$$

The final result expressed by equation (24) has been deduced neglecting the term $\mathrm{Re}^{-3/2}\,\mathrm{Oh}^{-2}$. This is done based on the fact that, in the regimes for which $\delta \sim H_a$, namely, $\mathrm{Re}^{1/6}\mathrm{Oh}^{2/3} \gtrsim 0.25$, the Ohnesorge number satisfies the condition $\mathrm{Oh} \gtrsim 0.03$ (see Table II). Therefore, for the usual range of Reynolds numbers for which millimetric droplets splash namely, $\mathrm{Re} \sim 10^2 - 10^3$, $\mathrm{Re}^{-3/2}\,\mathrm{Oh}^{-2} < 1$. Finally, it can be concluded that the ejection time t_e in the regime $\mathrm{Re}^{1/6}\mathrm{Oh}^{2/3} \gtrsim 0.25$ can be calculated as

$$\begin{aligned} \dot{v}_t = \ddot{a} &\Rightarrow -\mathrm{Re}^{-1/2} \propto \ddot{a}\,h_a^2 \propto -t_e^{3/2} \\ &\Rightarrow t_e \propto \mathrm{Re}^{-1/3}. \end{aligned} \tag{25}$$

Figure 8 shows good agreement between the ejection times predicted by equations (22) and (25) and the experimental ejection times reported in [1] and in [10]. Notice also that, while the ejection times predicted by equation (1) are also in good agreement with experiments for sufficiently low values of the Ohnesorge number, the deviations between the predictions of equation (1) and measurements are apparent for the case of higher viscosity fluids.

The thickening of the lamella provoked by the development of a boundary layer between the stagnation point and the root of the ejected sheet, can be approximately quantified imposing that the flow rate entering into the lamella coincides with that predicted by potential flow theory. Assuming a velocity profile within the boundary layer increasing linearly with the distance to the wall, the thickness of the root of the lamella, h_a^+ when the effect of the boundary layer is taken into account -see the sketch in figure 1-, is given by

$$\begin{aligned} h_a v_a &= v_a\left(h_a^+ - \frac{\delta}{R}\right) + \frac{\delta}{2R} v_a \\ \Rightarrow h_a^+ &\propto h_a\left(1 + 2.2/\sqrt{\mathrm{Re}\,t_e}\right), \end{aligned} \tag{26}$$

with δ given in equation (19) and h_a given by equation (2). In order to improve the agreement with experiments for the smaller values of the Reynolds number, and due to the fact that, in the limit $\sqrt{\mathrm{Re}\,t_e} \gg 1$, the result in equation (26) can be very well approximated by

$$h_a^+ \propto \frac{h_a}{1 - 2.2/\sqrt{\mathrm{Re}\,t_e}}, \tag{27}$$

we alternatively use here the following expression to calculate h_a^+:

$$h_a^+ = \frac{h_a}{1 - K_a/\sqrt{\mathrm{Re}\,t_e}}, \tag{28}$$

where K_a is a constant which will be determined by matching the predictions with the experimental data and whose precise value will be very close to our prediction in equation (27). In addition, to account for the thickening of the rim produced by the capillary retraction during the first instants after the ejection of the lamella (see the numerical shapes in Figure 2 for illustrative purposes), the thickness of the edge of the advancing lamella will be calculated here as

$$h_t = K_h h_a^+ = K_h \frac{h_a}{1 - K_a/\sqrt{\mathrm{Re}\,t_e}}, \tag{29}$$

a very similar expression to that suggested by the experiments in [1], where we found that $h_t \approx 2.8\,h_a$.

Figure 9 show the comparison between the experimental values of the splash threshold velocities satisfying the condition $\mathrm{Re}^{1/6}\mathrm{Oh}^{2/3} < 0.25$ and the theoretical ones, determined using

$$\left(\frac{F_L}{2\sigma}\right)^{1/2} = 0.14, \tag{30}$$

with F_L given by equation (3), t_e and h_t calculated through equations (22) and (29) respectively, $I_\mu = H_t\,\mu_g/\mu$, $K_a = 2.8$, and the same values for the rest of the parameters as in [1]: $v_t = \sqrt{3/2}\,t_e^{-1/2}$, $\alpha = 61^\circ$, $K_h = 2.5$ and $H_0 = H_t/4$.

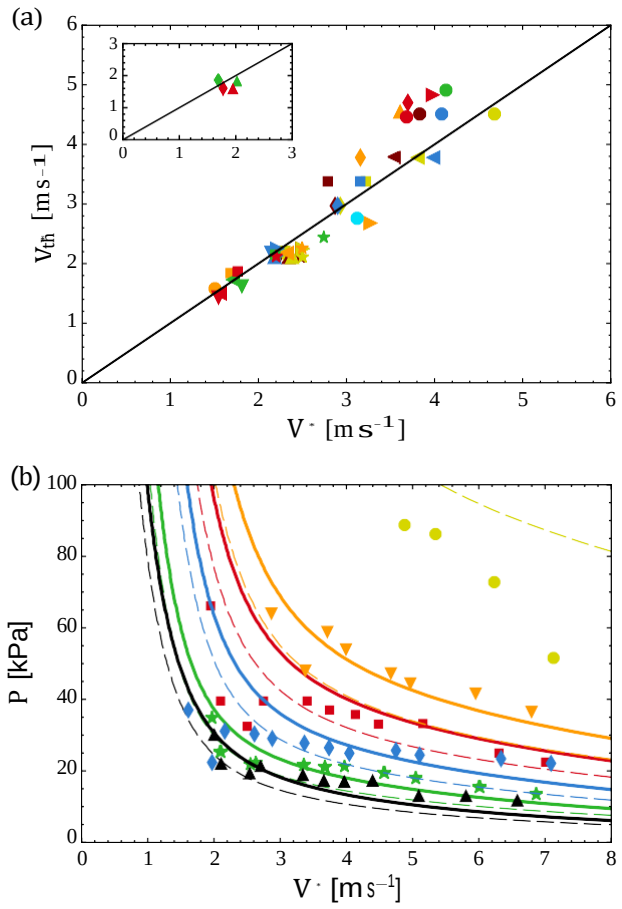

FIG. 9. (color online). (*a*) Comparison between the critical velocity V^* measured experimentally for the case $\mathrm{Re}^{1/6}\,\mathrm{Oh}^{2/3} < 0.25$ and the corresponding velocities predicted by equation (30). The material properties of the different liquids used, the type of solid substrate, the radii of the impacting drops and the corresponding values of the Ohnesorge number, are summarized in Table II. The inset represents the comparison between predicted and measured values of V^* when $\mathrm{Re}^{1/6}\,\mathrm{Oh}^{2/3} > 0.25$. In Figure (*a*), the surrounding gas is air at normal atmospheric conditions (see Table I). (*b*) Comparison between the predicted and measured values of the critical splash velocity for the case of the experiments reported in [5]. In this case, $\mathrm{Re}^{1/6}\,\mathrm{Oh}^{2/3} < 0.25$ and the material properties of the gases and liquids used are provided in Tables I and III respectively. Continuous lines represent the predicted value of V^* for $K_h = 2$ and the corresponding values of V^* for $K_h = 2.5$, are represented in dashed lines.

The agreement between the predicted velocities and the experimental ones is fairly good in view of the wide range of viscosities, drop diameters, values of the interfacial tension coefficient, different substrate wettabilities [20], different gases and different gas pressures considered [5], and this agreement can be even improved if the constant K_h is set to $K_h = 2$ in Figure 9(*b*). The splash threshold velocities for the case $\mathrm{Re}^{1/6}\mathrm{Oh}^{2/3} > 0.25$, which are calculated in the same way as before, but making use of equation (25) to calculate t_e, are also in good agreement with the experimental data, as the inset in Figure 9(*a*) shows.

Ref.	Symb.	ρ (kg/m^3)	σ (mN/m)	μ (cP)	V^* (m/s)	Re (-)	Oh ($\times 10^3$)	Type
(a) [1]	●	789	24.0	0.3	3.12	7677	2.4	G
(b) [1]	●	1000	71.8	0.95	3.68	7583	2.5	G
[1]	♦	1000	71.8	0.95	3.70	6760	2.7	G
[1]	▶	1000	71.8	0.95	3.98	6832	2.8	G
[1]	●	1000	67.5	0.9	4.13	6395	2.9	G
(c) [1]	★	791	23.5	0.6	2.20	4507	3.5	G
[1]	★	791	23.5	0.6	2.74	3878	4.2	G
(d) [1]	■	789	22.6	1.0	1.77	2130	6.1	G
[1]	■	789	22.6	1.0	2.19	1834	7.3	G
(e) [1]	◀	854	17.2	1.3	1.56	1400	9.1	G
[1]	◀	854	17.2	1.3	1.71	988	11.4	G
(f) [1]	▼	875	17.8	1.7	1.55	1062	12.0	G
[1]	▼	875	17.8	1.7	1.81	830	14.7	G
(g) [1]	♦	913	18.6	4.6	1.77	466	30.5	G
[1]	♦	913	18.6	4.6	1.69	313	37.1	G
(h) [1]	▲	1000	19.5	10.0	1.95	258	62.2	G
[1]	▲	1000	19.5	10.0	2.02	182	75.3	G
[20]	●	989	56.4	1.23	3.83	3394	5.0	P
[20]	◀	982	48.1	1.50	3.54	2548	6.6	P
[20]	■	975	42.7	1.82	2.79	1492	8.9	P
[20]	♦	969	38.0	2.14	2.87	1233	11.5	P
[20]	▶	935	30.2	2.85	2.50	738	17.9	P
[20]	★	891	26.2	2.55	2.48	694	18.6	P
[20]	▲	843	23.8	1.88	2.34	840	14.8	P
[20]	▼	789	21.8	1.20	2.26	1186	10.2	P
[20]	●	989	56.4	1.23	4.68	4146	5.0	G
[20]	◀	982	48.1	1.50	3.81	2740	6.6	G
[20]	■	975	42.7	1.82	3.22	1724	8.9	G
[20]	♦	969	38.0	2.14	2.93	1259	11.5	G
[20]	▶	935	30.2	2.85	2.50	739	17.9	G
[20]	★	891	26.2	2.55	2.50	700	18.6	G
[20]	▲	843	23.8	1.88	2.38	855	14.8	G
[20]	▼	789	21.8	1.20	2.28	1198	10.2	G
[20]	●	989	56.4	1.23	4.08	3615	5.0	S
[20]	◀	982	48.1	1.50	3.98	2868	6.6	S
[20]	■	975	42.7	1.82	3.15	1689	8.9	S
[20]	♦	969	38.0	2.14	2.90	1246	11.5	S
[20]	▶	935	30.2	2.85	2.21	654	17.9	S
[20]	★	891	26.2	2.55	2.21	619	18.6	S
[20]	▲	843	23.8	1.88	2.18	783	14.8	S
[20]	▼	789	21.8	1.20	2.15	1127	10.2	S
[15]	●	786	20.5	2.0	1.51	738	14.1	G
[15]	◀	805	22.3	1.38	2.32	1045	11.7	G
[15]	■	805	22.3	1.38	1.68	1271	9.1	G
[15]	♦	1050	60.0	1.78	3.16	3096	5.5	G
[15]	▶	792	22.2	0.52	3.27	3893	4.4	G
[15]	★	792	22.2	0.52	2.50	4576	3.6	G
[15]	▲	1000	70.8	1.00	3.61	6479	2.8	G

TABLE II. (color online) Values of the material properties of the liquids, values of critical velocity for splashing V^*, values of the corresponding Reynolds numbers $\mathrm{Re} = \rho R V^*/\mu$ as well as the Ohnesorge numbers $\mathrm{Oh} = \sqrt{\mathrm{We}}/\mathrm{Re} = \mu/\sqrt{\rho R \sigma}$ and type of solid substrate: G–Glass, P–Parafilm and S–Steel, used to plot Figure 9(*a*). (*a*) Acetone, (*b*) Water, (*c*) Methanol, (*d*) Ethanol, (*e*) Decamethyltetrasiloxane, (*f*) Dodecamethylpentasiloxane, (*g*) Poly(Dimethylsiloxane) and (*h*) 10 cP Silicone Oil.

Notice that, in the case of low viscosity liquids, and due to

Gas		ρ (kg/m³)	σ (mN/m)	μ (cP)	Oh ($\times 10^3$)	λ_0 (nm)	μ_g (cP)	ρ_{g0} (kg/m³)
(a)	●	789	22.4	1.04	6.0	180	0.0198	0.16
(b)	■	789	22.4	1.04	6.0	65	0.0185	1.18
(c)	★	789	22.4	1.04	6.0	55	0.0251	3.42
(d)	▲	789	22.4	1.04	6.0	39	0.0153	6.04
(*b*)	▼	791	23.5	0.54	3.0	65	0.0185	1.18
(*b*)	◆	786	21.0	2.04	12.2	65	0.0185	1.18

TABLE III. (color online) Values of the material properties of the liquids used in [5], reproduced in Figure 9(*b*), and values of the Ohnesorge numbers $\mathrm{Oh} = \sqrt{\mathrm{We}}/\mathrm{Re} = \mu/\sqrt{\rho R\sigma}$ corresponding to $R = 1.7$ mm. The material properties of the different gases used in the experiments reported in [5], (*a*) Helium, (*b*) Air, (*c*) Krypton and (*d*) SF_6, are provided in Table I.

the fact that $t_e \propto \mathrm{We}^{-2/3}$ and since $h_t \sim t_e^{3/2} \propto \mathrm{We}^{-1}$, the height of the advancing liquid sheet can reach values close to the mean free path of gas molecules. Indeed,

$$\frac{\lambda}{H_t} \sim \frac{\lambda}{R}\,\mathrm{We} = \mathrm{We}_\lambda = \frac{p_{g0}}{p_g}\frac{T_g}{T_{g0}}\,\mathrm{We}_{\lambda 0}, \qquad (31)$$

with $\mathrm{We}_\lambda = \rho V^2 \lambda/\sigma$ and λ_0 the mean free path at normal pressure and temperature conditions, p_{g0} and T_{g0} respectively. For instance, in the case of helium in Figure 9(*b*), $V^* \sim 5\ \mathrm{m\,s^{-1}}$, $\sigma \times 20 \times 10^{-3}\ \mathrm{N\,m^{-1}}$, $\rho \times 780\ \mathrm{kg\,m^{-3}}$, $\lambda_0 \times 180 \times 10^{-9}$ m and, therefore, $\mathrm{We}_\lambda \sim 0.2$. This result suggests that calculations of the type reported in [45, 46], are necessary to accurately predict the contribution of the gas lubrication layer to the lift force.

III. CONCLUDING REMARKS

The model developed in [1] has been completed by taking into account the effects associated with the growth of the boundary layer which, when the velocity field is described in a moving frame of reference, develops between the stagnation point of the flow and the root of the ejected liquid sheet. Depending on the value of the ratio δ/H_t, with δ the thickness of the boundary layer and H_t the initial thickness of the advancing rim, the ejection time is calculated either as $t_e \times 1.05\,\mathrm{We}^{-2/3}$ if $\mathrm{Re}^{1/6}\mathrm{Oh}^{2/3} < 0.25$, or as $t_e \times 0.6\,\mathrm{Re}^{-1/3}$ if $\mathrm{Re}^{1/6}\mathrm{Oh}^{2/3} > 0.25$. Interestingly enough, the predictions for the ejection times for the larger values of the Ohnesorge number, $t_e \propto \mathrm{Re}^{-1/3}$, which contrast with $t_e \propto \mathrm{Re}^{-1/2}$ in [1], are in better agreement with the experimental measurements. The predicted splash velocities are in fairly good agreement with experiments when both the modified ejection time and the thickening of the ejected lamella caused by the growth of the boundary layer, are included into the splash criterion $(F_L/2\sigma)^{1/2} = 0.14$, deduced in [1].

ACKNOWLEDGMENTS

This work has been supported by the Spanish MINECO under Projects DPI201459292-C3-2-P and DPI2015-71901-REDT, partly financed through European funds.

[1] G. Riboux and J. M. Gordillo, Phys. Rev. Lett. **113**, 024507 (2014).
[2] C. Josserand and S. T. Thoroddsen, Annu. Rev. Fluid Mech. **48**, 365 (2016).
[3] S. Brodbeck, Journal for Police Science and Practice **2**, 51 (2012).
[4] C. Mundo, M. Sommerfeld, and C. Tropea, Int. J. Multiphase Flow **21**, 151 (1995).
[5] L. Xu, W. W. Zhang, and S. R. Nagel, Phys. Rev. Lett. **94**, 184505 (2005).
[6] S. Mandre, M. Mani, and M. P. Brenner, Phys. Rev. Lett. **102**, 134502 (2009).
[7] L. Duchemin and C. Josserand, Phys. Fluids **23**, 091701 (2011).
[8] J. M. Kolinski, S. M. Rubinstein, S. Mandre, M. P. Brenner, D. A. Weitz, and L. Mahadevan, Phys. Rev. Lett. **108**, 074503 (2012).
[9] S. Thoroddsen, T. Etoh, T. K., N. Ootsuka, and Y. Hatsuki, J. Fluid Mech. **545**, 203212 (2005).
[10] S. Thoroddsen, K. Takehara, and T. G. Etoh, J. Fluid Mech. **706**, 560 (2012).
[11] J. C. Bird, S. S. H. Tsai, and H. A. Stone, New J. Phys. **11**, 063017 (2009).
[12] R. Rioboo, M. Marengo, and C. Tropea, Exp. Fluids **33**, 112 (2002).
[13] A. Yarin, Ann. Rev. Fluid Mech. **38**, 159 (2006).
[14] C. W. Visser, P. H. Frommhold, S. Wildeman, R. Mettin, D. Lohse, and C. Sun, Soft Matter **11**, 1708 (2015).
[15] J. Palacios, J. Hernandez, P. Gomez, C. Zanzi, and J. Lopez, Exp. Therm. Fluid Sci. **44**, 571582 (2013).
[16] C. S. Stevens, Europhys. Lett. **106**, 24001 (2014).
[17] J. Philippi, P. Y. Lagree, and A. Antkowiak, J. Fluid Mech. **795**, 96 (2016).
[18] C. J. Howland, A. Antkowiak, J. R. Castrejo´n-Pita, S. D. Howison, J. M. Oliver, R. W. Style, and A. A. Castrejo´n-Pita, Phys. Rev. Lett. **117**, 184502 (2016).
[19] H. J. J. Staat, T. Tran, B. Geerdink, G. Riboux, C. Sun, J. M. Gordillo, and D. Lohse, J. Fluid Mech. **779**, R3 (2015).
[20] T. C. Goede, K. G. de Bruin, and D. Bonn, arxivs (2017).
[21] J. Hao and S. I. Green, Phys. Fluids **29**, 012103 (2017).
[22] S. Thoroddsen, J. Fluid Mech. **451**, 373 (2002).
[23] F. T. Smith, L. Li, and G. X. Wu, J. Fluid Mech. **482**, 291 (2003).
[24] C. Josserand and S. Zaleski, Phys. Fluids **15**, 1650 (2003).
[25] A. Korobkin, S. Ellis, and F. Smith, J. Fluid Mech. **611**, 365 (2008).
[26] P. D. Hicks and R. Purvis, J. Fluid Mech. **649**, 135 (2010).
[27] L. V. Zhang, J. Toole, K. Fezzaa, , and R. D. Deegan, J. Fluid Mech. **703**, 402 (2012).

[28] Y. Scolan and A. Korobkin, J. Fluid Struct. **17**, 275 (2003).
[29] H. Wagner, Z. Angew. Math. Mech. **12**, 193 (1932).
[30] S. Howison, J. Ockendon, and S. Wilson, J. Fluid Mech. **222**, 215 (1991).
[31] S. Wilson, J. Engn. Maths. **25**, 265 (1991).
[32] J. M. Oliver, *Water Entry and Related Problems* (Thesis, Oxford Univ., 2002).
[33] P. D. Hicks and R. Purvis, J. Fluid Mech. **735**, 120 (2013).
[34] J. Maurer, P. Tabeling, P. Joseph, and H. Willaime, Phys. Fluids **15**, 2613 (2003).
[35] G. I. Taylor, Proc. R. Soc. A **253**, 296 (1959).
[36] F. E. C. Culick, J. Appl. Phys. **31**, 1128 (1960).
[37] G. Riboux and J. M. Gordillo, J. Fluid Mech. **803**, 516 (2016).
[38] I. V. Roisman, E. Berberovic´, and C. Tropea, Phys. Fluids **21**, 052103 (2009).
[39] I. V. Roisman, Phys. Fluids **21**, 052104 (2009).
[40] J. Eggers, M. Fontelos, C. Josserand, and S. Zaleski, Phys. Fluids **22**, 062101 (2010).
[41] S. Tabakova, F. Feuillebois, A. Mongruel, D. V., and S. Radev, Z. Angew. Math. Phys. **63**, 313 (2011).
[42] G. Riboux and J. M. Gordillo, J. Fluid Mech. **772**, 630 (2015).
[43] H. Schlichting, *Boundary-Layer Theory* (Mac Graw Hill, Seventh Edition, 1987).
[44] K. Chen and P. Libby, J. Fluid Mech. **33**, 273 (1968).
[45] J. Li, Phys. Rev. Lett. **117**, 214502 (2016).
[46] J. E. Sprittles, Phys. Rev. Lett. **118**, 114502 (2017).